

Formation of GW230529 from Isolated Binary Evolution and Its Electromagnetic Counterparts

JIN-PING ZHU ^{1,2,*}, RUI-CHONG HU ^{3,4,*}, YACHENG KANG ^{5,6}, BING ZHANG ^{3,4}, HUI TONG ^{1,2}, LIJING SHAO ^{6,7}
AND YING QIN ⁸

¹*School of Physics and Astronomy, Monash University, Clayton Victoria 3800, Australia*

²*OzGrav: The ARC Centre of Excellence for Gravitational Wave Discovery, Australia*

³*Nevada Center for Astrophysics, University of Nevada, Las Vegas, NV 89154, USA*

⁴*Department of Physics and Astronomy, University of Nevada, Las Vegas, NV 89154, USA*

⁵*Department of Astronomy, School of Physics, Peking University, Beijing 100871, China*

⁶*Kaoli Institute for Astronomy and Astrophysics, Peking University, Beijing 100871, China*

⁷*National Astronomical Observatories, Chinese Academy of Sciences, Beijing 100012, China*

⁸*Department of Physics, Anhui Normal University, Wuhu, Anhui 241002, China*

ABSTRACT

In this *Letter*, we explore the formation of the mass-gap black hole-neutron star (mgBHNS) merger detected in gravitational wave (GW) event, i.e., GW230529, from the isolated binary evolution channel, and study potential signatures of its electromagnetic signals. By adopting the ‘delayed’ supernova prescription and reasonable model realizations, our population synthesis simulation results can simultaneously match the inferred event rate densities of GW230529-like mgBHNS and total BHNS mergers, as well as the population distribution of the BH mass in BHNS mergers reported by the LIGO-Virgo-KAGRA Collaboration. Thus, we conclude that the recently-discovered mgBHNS merger, GW230529, can be explained through the isolated binary evolution channel. Considering the equation of states of AP4 and DD2, the probabilities that GW230529 can make tidal disruption are 12.8% and 63.2%, respectively. If GW230529 is a disrupted event, the associated kilonova is predicted to have an apparent magnitude of $\sim 23 - 24$ mag, and hence, can be detected by the present survey projects and LSST. Since GW230529 could be an off-axis event inferred from the GW observation, its associated gamma-ray burst (GRB) might be too dim to be observed by γ -ray detectors, interpreting the lack of GRB observations. The detection of GW230529 confirms the existence of mgBHNS mergers formed through the isolated binary evolution channel, suggesting that BHNS mergers are still likely to be multimessenger sources that emit GWs, GRBs, and kilonovae. Although mgBHNS mergers account for $\sim 60\%$ cosmological BHNS population, we find that $\gtrsim 90\%$ disrupted BHNS mergers are expected to originate from mgBHNS mergers.

Keywords: Gravitational waves (678); Neutron stars (1108); Black holes (162)

1. INTRODUCTION

Black hole–neutron star (BHNS) mergers are prime search targets for the ground-based gravitational-wave (GW) detectors, including LIGO (LIGO Scientific Collaboration et al. 2015), Virgo (Acernese et al. 2015), and KAGRA (Aso et al. 2013). Until the end of the GW third observing run (O3), the first two BHNS mergers

were identified by the LIGO-Virgo-KAGRA (LVK) Collaboration (Abbott et al. 2021a), with GW200105 being a merger between a $8.9^{+1.2}_{-1.5} M_{\odot}$ BH and a $1.9^{+0.3}_{-0.2} M_{\odot}$ NS, and GW200115 being a merger between a $5.7^{+1.8}_{-2.1} M_{\odot}$ BH and a $1.5^{+0.7}_{-0.3} M_{\odot}$ NS. During O3, the LVK Collaboration reported three additional marginal BHNS candidates (Abbott et al. 2021b; The LIGO Scientific Collaboration et al. 2021; Abbott et al. 2023), with GW190426_152155 involving a $5.7^{+3.9}_{-2.3} M_{\odot}$ BH and a $1.5^{+0.8}_{-0.5} M_{\odot}$ NS, GW190917_114630 involving a $9.7^{+3.4}_{-3.9} M_{\odot}$ BH and a $2.1^{+1.1}_{-0.4} M_{\odot}$ NS, as well as GW191219_163120 involving a $31.1^{+2.2}_{-2.8} M_{\odot}$ BH and a $1.17^{+0.07}_{-0.06} M_{\odot}$ NS. GWTC-3 also includes a puzzling GW event, GW190814, composed of

Corresponding author: Jin-Ping Zhu, Rui-Chong Hu, Bing Zhang
jin-ping.zhu@monash.edu, ruichong.hu@unlv.edu,
bing.zhang@unlv.edu

* These authors contributed equally to this work

a $22.2 - 24.3 M_{\odot}$ primary BH and a $2.50 - 2.67 M_{\odot}$ secondary compact object (Abbott et al. 2020). The origin of its secondary object is unclear, which could be either a low-mass BH or a massive NS. The LVK Collaboration also discovered a similar, but marginal GW candidate, namely GW200210.092254 (Abbott et al. 2023), with component masses inferred to be $24.1^{+7.5}_{-4.6} M_{\odot}$ and $2.83^{+0.47}_{-0.42} M_{\odot}$, respectively.

The X-ray and radio observations of Galactic pulsars implied a likely NS maximum mass of $\sim 2 - 2.3 M_{\odot}$ (e.g., Antoniadis et al. 2013; Alsing et al. 2018; Romani et al. 2022) while Galactic BHs in X-ray binaries were inferred to have a lower boundary close to $\sim 5 M_{\odot}$ (Bailyn et al. 1998; Özel et al. 2010; Farr et al. 2011), leading to the conjecture of the presence of a mass gap between the heaviest NSs and lightest BHs. However, recent electromagnetic (EM) observations of non-interacting binary systems (Thompson et al. 2019; Rivinius et al. 2020; Andrews et al. 2022) and gravitational microlensing events (Wyrzykowski & Mandel 2020) indicated that the mass gap might be partially polluted. The population properties of O3 BHNS candidates suggested a relative dearth of events with masses in the mass gap (Zhu et al. 2022b; Ye & Fishbach 2022; Biscoveanu et al. 2023), which was also supported by the population study on merging compact binaries in GWTC-3 (Abbott et al. 2023). Whether there is a mass gap or not can shed light on supernova (SN) mechanisms for the formation of NSs and BHs, with the rapid model giving rise to the mass gap, while the delayed model does not (Fryer et al. 2012). Population synthesis simulations revealed that BHs in $\sim 30 - 80\%$ BHNS mergers can have a mass in the mass gap by considering the delayed SN model (Shao & Li 2021; Drozda et al. 2022). It is expected that future detection of merging mass-gap BHNS (mgBHNS) binaries through GW observations can give a better constraint on the SN mechanisms.

Binary NSs (BNSs) and BHNSs have long been proposed to be progenitors of some fast-evolving EM transients, including gamma-ray bursts (GRBs; Paczynski 1986, 1991; Eichler et al. 1989; Narayan et al. 1992; Zhang 2018; Gottlieb et al. 2023) and kilonovae (Li & Paczyński 1998; Metzger et al. 2010). While BNS mergers were confirmed as the origin of GRBs and kilonovae thanks to the associations between GW170817 (Abbott et al. 2017a), GRB170817A (Abbott et al. 2017b; Goldstein et al. 2017; Savchenko et al. 2017; Zhang et al. 2018), and AT2017gfo (e.g., Abbott et al. 2017c; Arcavi et al. 2017; Coulter et al. 2017; Drout et al. 2017; Evans et al. 2017; Kasen et al. 2017; Kasliwal et al. 2017; Kilpatrick et al. 2017; Pian et al. 2017; Smartt et al. 2017), the joint observations of the O3 BHNS GW

candidates and their associated EM counterparts, especially for kilonova emissions, were absent. One possible reason for the lack of kilonova detection following O3 BHNS GW signals could be the challenge of rapidly achieving full distance and volumetric coverage for the probability maps of the LVK Collaboration within the short kilonova duration by current survey projects (e.g., Coughlin et al. 2020; Kasliwal et al. 2020; Gompertz et al. 2020; Anand et al. 2021). Unlike BNS mergers, which typically eject a certain amount of materials to produce EM counterparts, the NS components in some merging BHNS binaries may directly plunge into their BH companions without generating any observable EM signals. NS tidal disruption tends to occur if the BHNS binaries have a low-mass BH with a high orbital aligned spin and a low-mass NS with a stiff EoS (Shibata & Taniguchi 2011; Foucart 2012; Kyutoku et al. 2013, 2015; Kawaguchi et al. 2016; Foucart et al. 2018; Zhu et al. 2020, 2021b; Hayashi et al. 2021; Sarin et al. 2022). More specifically, since primary BHs (produced from initially more massive star) formed through the classical common envelope scenario typically possess near-zero aligned spins (Qin et al. 2018; Fuller et al. 2019; Belczynski et al. 2020), tidal disruptions of most cosmological BHNS mergers are expected to occur if the BHs have a mass of $\lesssim 6 - 7 M_{\odot}$ and the NSs have a mass of $\lesssim 1.5 M_{\odot}$ (e.g., Zhu et al. 2021a, 2022b). If the mass gap does exist, the mass space that allows NS tidal disruption and produces bright EM signals could be limited. Because O3 BHNS candidates have BH masses of $\gtrsim 5 M_{\odot}$ inferred from GW observations, their posterior mass distributions mostly lie outside the tidal disruption mass range (Abbott et al. 2021a; Zhu et al. 2021a, 2022b; D’Orazio et al. 2022). Thus, it is likely that the EM counterparts associated with these BHNS candidates were intrinsically missing. Additionally, although a few O3 BHNS candidates still have low probabilities of undergoing tidal disruption and producing kilonova emissions, the brightness of these kilonovae might be too dim to be detected by current survey telescopes due to their remote distance from us (Zhu et al. 2021a).

The discovery of mgBHNS mergers through GW observations can provide an opportunity to constrain SN mechanisms and isolated formation channel of compact binaries. Furthermore, mgBHNS mergers are more likely to have tidal disruption and produce observable EM counterparts. Multimessenger observations of BHNS mergers between GWs and EMs can be more easily achieved if mgBHNS mergers exist. Most recently, the LVK Collaboration reported the first mgBHNS merger, GW230529, detected in the first part of the fourth observing run (The LIGO Scientific Collabo-

ration et al. 2024). By adopting the combined posterior results inferred by the low-spin prior of the secondary component (The LIGO Scientific Collaboration et al. 2024), the primary BH mass of GW230529 is $M_{\text{BH}} = 3.6_{-1.2}^{+0.7} M_{\odot}$ nearly filling in the mass gap, while its secondary NS mass is $M_{\text{NS}} = 1.43_{-0.19}^{+0.59} M_{\odot}$. The effective inspiral-spin and effective precessing-spin of GW230529 are $\chi_{\text{eff}} = -0.10_{-0.17}^{+0.10}$ and $\chi_{\text{p}} = 0.40_{-0.34}^{+0.37}$, respectively. The source has a redshift of $z = 0.043_{-0.021}^{+0.023}$, corresponding to a luminosity distance of $D_{\text{L}} = 197_{-96}^{+107}$ Mpc. The LIGO Scientific Collaboration et al. (2024) gave the rate density of $\mathcal{R}_{230529} = 55_{-47}^{+127} \text{Gpc}^{-3} \text{yr}^{-1}$ for compact object coalescences with properties similar to GW230529. Similar to the estimation of \mathcal{R}_{230529} , they also updated a total BHNS rate density to $\mathcal{R}_{\text{BHNS}} = 85_{-57}^{+116} \text{Gpc}^{-3} \text{yr}^{-1}$ by including the other two O3 BHNS mergers (GW200105 and GW200115)¹. In this *Letter*, we explore the formation of GW230529 through the isolated binary evolution channel and study the properties of its associated EM counterparts.

2. POPULATION SYNTHESIS OF BHNS MERGERS AND FORMATION OF GW230529

2.1. Method

In this section, we employ the rapid binary population synthesis code COMPAS (Stevenson et al. 2017; Vigna-Gómez et al. 2018; Neijssel et al. 2019; Team COMPAS: Riley, J. et al. 2022) to explore the formation of GW230529 through the isolated binary evolution channel. To characterize star formation environments, we adopt a metallicity-specific star formation rate density model suggested in Broekgaarden & Berger (2021) which combines the Madau & Dickinson (2014) star formation density with the Panter et al. (2004) mass-metallicity relation. To determine compact object masses during core-collapse SNe of stars, the ‘delayed’ SN prescription (Fryer et al. 2012) is adopted, which allows for the production of mass-gap BHs (see also Mandel & Müller 2020). Based on the metallicity-specific star formation rate density prescription, we generate and evolve binary systems according to the fiducial population synthesis model described in Table 1 of Broekgaarden et al. (2021), with the maximum NS mass changed to $M_{\text{NS,max}} = 2.2 M_{\odot}$, and the velocity dispersion of BH natal kick, modeled with a Maxwellian distribution, to $\sigma_{\text{BH}} = 100 \text{ km s}^{-1}$ following with the measurements on

¹ By considering that GW200105, GW200115, and GW230529 belong to a single population class, as well as taking into account some marginal events detected before GW230529, The LIGO Scientific Collaboration et al. (2024) also gave another BHNS rate density of $\mathcal{R}_{\text{BHNS}} = 94_{-64}^{+109} \text{Gpc}^{-3} \text{yr}^{-1}$.

Table 1. Merger Rate Density of Population Synthesis Simulation

Model	\mathcal{R}_{230529} ($\text{Gpc}^{-3} \text{yr}^{-1}$)	$\mathcal{R}_{\text{BHNS}}$ ($\text{Gpc}^{-3} \text{yr}^{-1}$)	CI
$\alpha 1\sigma 100$	65	180	0.64
$\alpha 2\sigma 100$	58	146	0.38
$\alpha 5\sigma 100$	47	74	0.09
$\alpha 10\sigma 100$	54	71	0.13
$\alpha 1\sigma 265$	41	134	0.29
$\alpha 2\sigma 265$	49	115	0.09
$\alpha 5\sigma 265$	37	60	0.36
$\alpha 10\sigma 265$	34	52	0.50

NOTE—The columns are (1) the population synthesis model; (2) the simulated local merger rate density of GW230529-like events in $\text{Gpc}^{-3} \text{yr}^{-1}$; (3) the simulated local merger rate density of total BHNS mergers in $\text{Gpc}^{-3} \text{yr}^{-1}$; (4) the credible interval.

the proper motions of Galactic BH X-ray binaries (Atri et al. 2019).

We explore the variations of different common envelope efficiencies ($\alpha_{\text{CE}} = 1, 2, 5, 10$) and velocity dispersions of NS natal kicks ($\sigma_{\text{NS}} = 100, 265 \text{ km s}^{-1}$; Hobbs et al. 2005) in the formation of BHNS mergers. The naming convention of our population synthesis models follows the pattern $\alpha X \sigma Y$, where X and Y are the corresponding values of α_{CE} and σ_{NS} . Totally, our population synthesis simulations include 8 models, each evolving 10^6 binaries from the zero-age main sequence stage. We select BHNS merger systems if the final primary mass $M_1 > M_{\text{NS,max}}$ and secondary mass $M_2 < M_{\text{NS,max}}$, while we identify GW230529-like systems if both M_1 and M_2 lie within the inferred 90% credible intervals of GW230529.

2.2. Results

The simulated local event rate densities of GW230529-like events and BHNS mergers are listed in Table 1 and are displayed in Figure 1. Based on the probability density functions of \mathcal{R}_{230529} and $\mathcal{R}_{\text{BHNS}}$, assuming they are independent, we calculate the credible interval of our population synthesis simulations for the LVK’s observations. The event rate densities of our population synthesis simulations are all within the 60% credible intervals of observed \mathcal{R}_{230529} and $\mathcal{R}_{\text{BHNS}}$. We find that the models with a lower common-envelope efficiency ($\alpha_{\text{CE}} \lesssim 2$) indicates a better agreement with the LVK’s observations when the natal kick is strong ($\sigma_{\text{NS}} = 265 \text{ km s}^{-1}$),

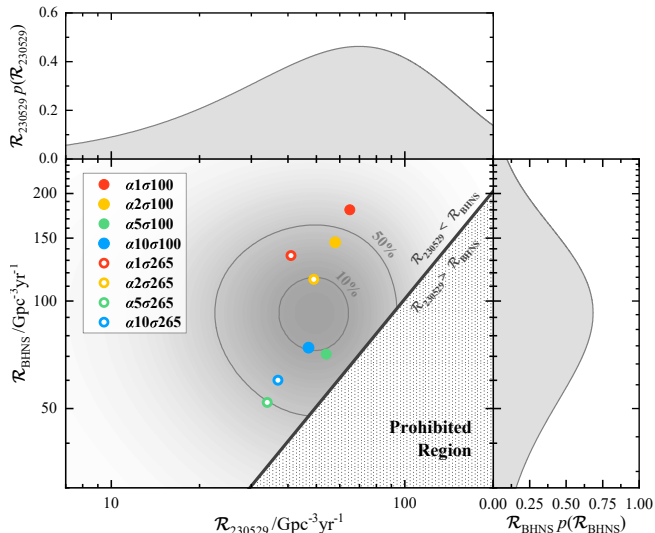


Figure 1. Simulated local rate density of GW230529-like event and BHNS mergers. The red, orange, green, and blue points correspond to different envelope efficiencies of $\alpha_{\text{CE}} = 1, 2, 5,$ and $10,$ respectively. The solid and hollow points represent two NS natal kicks of $\sigma_{\text{NS}} = 100$ and 265 km s^{-1} . The top and right panels display the posteriors on the merger rate densities of GW230529-like events and BHNS mergers obtained from [The LIGO Scientific Collaboration et al. \(2024\)](#). The 10% and 50% credible interval regions of the posteriors are marked as solid gray lines. The shadow region in the bottom right represents the prohibited parameter space where $\mathcal{R}_{230529} > \mathcal{R}_{\text{BHNS}}$.

whereas those with higher common-envelope efficiency ($\alpha_{\text{CE}} \gtrsim 5$) suggests better consistency with the observations when the kick velocity is relatively low ($\sigma_{\text{NS}} = 100 \text{ km s}^{-1}$). Among these population synthesis models, the models of $\alpha 5\sigma 100$ and $\alpha 2\sigma 265$, exhibit credible intervals lower than 10% within the GW observations.

By combining the population synthesis simulation results of $\alpha 5\sigma 100$ and $\alpha 2\sigma 265$, we show the distribution of the BH mass and NS mass for simulated BHNS population in Figure 2. The medians with the 90% credible intervals of the inferred posterior samples for GW200115, GW200105, and GW230529 are also displayed. One can find that the combined model predicts that the majority of BHNS mergers can have a BH mass of $2.2 - 11 M_{\odot}$, and a NS mass of $1.25 - 2.2 M_{\odot}$, with a concentration of $\sim 1.3 M_{\odot}$. The inferred properties of GW200105, GW200115, and GW230529 lie within the 90% credible interval of our simulated BHNS population. In particular, the medians with a large fraction of the posterior for the mgBHNS event, i.e., GW230529, recently reported by the LVK Collaboration significantly overlap with the highest probability region of the simulated BHNS population. We find that the predicted BH mass distribution is basically consistent with that of GW BHNS pop-

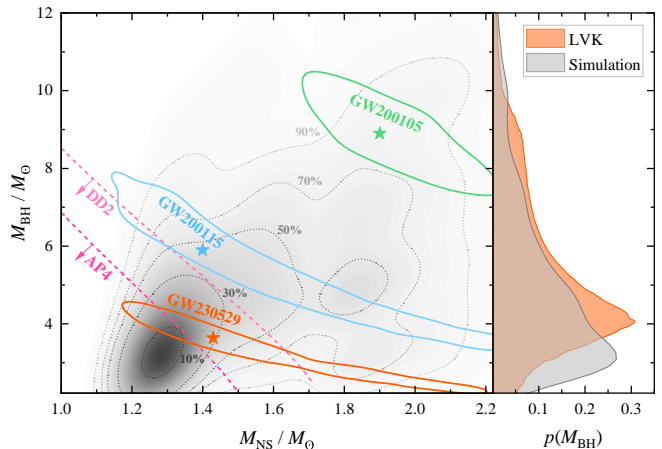


Figure 2. NS and BH masses of our population synthesis simulations. The grey dotted lines represent the credible interval regions of the simulation results, spanning from 10% to 90%, estimated using kernel density estimation. The medians (star points) along with their corresponding 90% credible intervals (solid lines) are illustrated for the posterior distributions of GW200105 (green), GW200115 (blue), and GW230529 (orange). The right panel shows the population distribution of the BH mass inferred by the GW observations (orange histogram; [The LIGO Scientific Collaboration et al. 2024](#)), contrasted with that derived from our population synthesis simulations (grey histogram). For an EoS of AP4 (DD2), non-spinning BHNS mergers with component masses located at the bottom left parameter space of the pink (light pink) dashed line can allow tidal disruption.

ulation inferred by the presently detected three high-confidence BHNS mergers, particularly for the mass space of $\gtrsim 5 M_{\odot}$. Compared with the present GW observation, where the BH mass peaks at $\sim 4 M_{\odot}$, our simulated BH population has a lower mass peak of $3.2 M_{\odot}$.

Overall, our population synthesis simulation results can simultaneously match the inferred event rate densities of GW230529-like mgBHNS and total BHNS mergers, along with the GW population distribution of the BH mass in BHNS mergers. The posterior masses of GW230529 given by the LVK Collaboration are close to the highest probability region of the simulated BHNS population. Therefore, one can expect that GW230529 can likely originate from the isolated binary evolution channel.

3. EM COUNTERPARTS OF GW230529 AND IMPLICATIONS FOR FUTURE BHNS EM OBSERVATIONS

GW230529 was only observed by LIGO Livingston and, hence, had a sky localization with a 90% credible area of $\sim 25600 \text{ deg}^2$ ([The LIGO Scientific Collaboration et al. 2024](#)), which was too wide for follow-up observations. There were no kilonova and GRB candi-

dates reported after this event. In this section, we will study the tidal disruption probability and EM signals of GW230529. Furthermore, with the discovery of the existence of mgBHNS mergers, our previous understanding of the detectability of BHNS EM signals may change. We will also briefly explore the future detectability of BHNS EM signals based on our population synthesis simulations.

3.1. Tidal Disruption Probability

Whether tidal disruption can occur in a BHNS merger can be described by an empirical formula (Foucart et al. 2018)

$$\frac{M_{\text{total,fit}}}{M_{\text{NS}}^{\text{b}}} = \left[\max \left(\alpha \frac{1 - 2C_{\text{NS}}}{\eta^{1/3}} - \beta \tilde{R}_{\text{ISCO}} \frac{C_{\text{NS}}}{\eta} + \gamma, 0 \right) \right]^{\delta}, \quad (1)$$

which is used to calculate the total remnant mass outside the remnant BH horizon, where $\alpha = 0.406$, $\beta = 0.139$, $\gamma = 0.255$, $\delta = 1.761$, M_{NS}^{b} is the baryonic NS mass, $\eta = Q/(1+Q)^2$, $Q = M_{\text{BH}}/M_{\text{NS}}$ is the mass ratio between the BH mass M_{BH} and the NS mass M_{NS} , $C_{\text{NS}} = GM_{\text{NS}}/c^2 R_{\text{NS}}$ is the compactness dependent on the NS equation of state (EoS) with the gravitational constant G , speed of light c , and NS radius R_{NS} . The normalized inner stable circular orbit radius (Bardeen et al. 1972) can be expressed as $\tilde{R}_{\text{ISCO}} = 3 + Z_2 - \text{sign}(\chi_{\text{BH},z})\sqrt{(3 - Z_1)(3 + Z_1 + 2Z_2)}$, where $Z_1 = 1 + (1 - \chi_{\text{BH},z}^2)^{1/3}[(1 + \chi_{\text{BH},z})^{1/3} + (1 - \chi_{\text{BH},z})^{1/3}]$, $Z_2 = \sqrt{3\chi_{\text{BH},z}^2 + Z_1^2}$, and $\chi_{\text{BH},z}$ is the dimensionless spin parameter projected onto the orientation of orbital angular momentum, abbreviated as the BH aligned-spin hereafter. This formula can be more accurately applied in the range of $Q \in [1, 7]$, $\chi_{\text{BH}} \in [-0.5, 0.9]$, and $C_{\text{NS}} \in [0.13, 0.182]$ (Foucart et al. 2018). BHNS mergers with component masses located in the parameter space of $M_{\text{total}} > 0$ can undergo tidal disruption and generate EM signals.

We consider two specific EoSs commonly used in the literature, among which AP4 (Akmal & Pandharipande 1997) is one of the most probable EoSs with a Tolman-Oppenheimer-Volkoff mass of $M_{\text{TOV}} = 2.22 M_{\odot}$, while DD2 (Typel et al. 2010) is one of the stiffest EoSs constrained by GW170817 (Abbott et al. 2018a, 2019), with $M_{\text{TOV}} = 2.42 M_{\odot}$. We calculate the baryonic NS mass in Equation (1) as follow: $M_{\text{NS}}^{\text{b}} = M_{\text{NS},\odot} + A_1 \times M_{\text{NS},\odot}^2 + A_2 M_{\text{NS},\odot}^3$, where $M_{\text{NS},\odot} = M_{\text{NS}}/M_{\odot}$, and we adopt the fitting values $A_1 = 0.045$ (0.046) and $A_2 = 0.023$ (0.014) for an EoS of AP4 (DD2) from Gao et al. (2020). The NS compactness is given by the fitting formula from Coughlin et al. (2017), i.e., $C_{\text{NS}} = 1.1056 \times (M_{\text{NS}}^{\text{b}}/M_{\text{NS}} - 1)^{0.8277}$.

Figure 3 shows the parameter space where the NS can be tidally disrupted using Equation (1). For a given $\chi_{\text{BH},z}$, BHNS mergers composed of a low-mass BH component and a low-mass NS component are more easily to have tidal disruption. The mass space that allows NS tidal disruption expands significantly with increasing $\chi_{\text{BH},z}$ and the adoption of a stiffer EoS. We display the 90% credible posterior distributions and the medians of component masses, as well as the medians of BH aligned-spins $\chi_{\text{BH},z}$, for GW200105, GW200115, and GW230529 (Abbott et al. 2021a; The LIGO Scientific Collaboration et al. 2024) in Figure 3. The explicit results of the tidal disruption probabilities for these three BHNS mergers are listed in Table 2. It is obvious that GW200105 is unlikely to make tidal disruption to generate any EM counterparts, because its BH and NS components are massive with the mass distribution significantly outside the tidal disruption region. Although GW200115 has BH and NS masses much lighter than those of GW200105, tidal disruption can occur with only a very low probability of $P_{\text{tidal}} = 2.76\%$ under the EoS of DD2. Compared with GW200105 and GW200115 whose BH masses are $\gtrsim 5 M_{\odot}$, GW230529, as a mgBHNS merger, occupies a larger portion of its mass parameter space located within the disruption region, especially when considering a stiffer EoS. More specifically, the tidal disruption probabilities are 12.8% and 63.2% by adopting the EoS of AP4 and DD2, respectively. The former value is similar to that reported in The LIGO Scientific Collaboration et al. (2024), which was obtained by marginalizing over the EoS.

3.2. Kilonova Properties

Tidal disruption of a BHNS merger can directly generate unbound lanthanide-rich dynamical ejecta, while other unswallowed material can form a disk around the remnant BH. Based on Zhu et al. (2020), one can calculate the mass of the dynamical ejecta by $M_{\text{d}} = \min(f_{\text{max}} M_{\text{total,fit}}, M_{\text{d,fit}})$ and disk mass by $M_{\text{disk}} = M_{\text{tot,fit}} - M_{\text{d}}$, where f_{max} represents the maximum fraction of the dynamical ejecta mass in the total remnant mass as determined by the numerical relativity simulations (Kyutoku et al. 2015) and $M_{\text{d,fit}}$ can be obtained by substituting the fitting parameters in Equation (1) with $\alpha = 0.273$, $\beta = 0.035$, $\gamma = -0.153$ and $\delta = 1.491$. The root-mean-square velocity of the dynamical ejecta can be described by $v_{\text{rms,d}} = (-0.441Q^{-0.224} + 0.549)c$, which is applied for $Q \in [1, 7]$. In addition to the tidal dynamical ejecta, the remnant disk can also produce lanthanide-free neutrino-driven wind ejecta caused by neutrino heating and intermediate-opacity viscosity-driven wind ejecta due to viscous heating and angu-

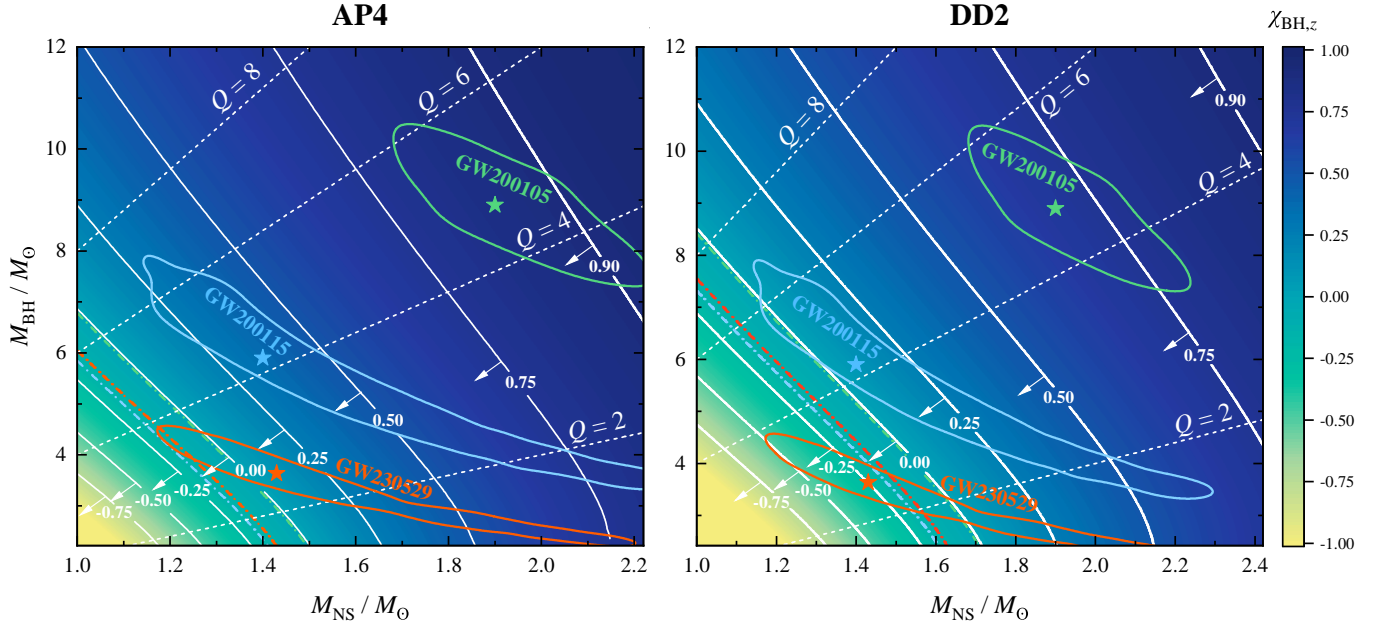


Figure 3. Source-frame mass parameter space for BHNS merger systems to allow NS tidal disruption. We mark the mass ratio from $Q = 2$ to 8 as dashed lines in each panel. The solid lines represent the primary BH aligned-spin $\chi_{\text{BH},z}$ from -0.75 to 0.90 . For a specific $\chi_{\text{BH},z}$, BHNS mergers with component masses located at the bottom left parameter space (denoted by the direction of the arrows) can undergo tidal disruption. For GW200105 (green), GW200115 (blue), and GW230529 (orange), the 90% credible posterior distributions (colored solid lines) and the medians (colored stars) are displayed, while the corresponding median values of $\chi_{\text{BH},z}$ for these three sources are marked as dashed-dotted lines.

Table 2. Tidal Disruption Probability, Kilonova Brightness, and GRB Detection Probability of BHNS Mergers

GW Event	EoS	P_{tidal}	m_g/mag	m_r/mag	P_{GRB}	
					$\theta_c = 3.5^\circ$	$\theta_c = 7^\circ$
GW200105	AP4	0%	—	—	—	—
	DD2	0%	—	—	—	—
GW200115	AP4	0%	—	—	—	—
	DD2	2.76%	$24.5^{+1.1}_{-1.3}$	$24.4^{+1.3}_{-1.1}$	0.004%	0.004%
GW230529	AP4	12.8%	$24.4^{+1.5}_{-1.9}$	$24.3^{+1.7}_{-1.9}$	0.35%	0.77%
	DD2	63.2%	$23.4^{+1.6}_{-1.3}$	$23.2^{+1.6}_{-1.4}$	1.56%	4.61%

NOTE—The columns are (1) the GW event; (2) the selected EoS; (3) the tidal disruption probability; (4) the median values with 90% credible intervals of g -band apparent magnitude distribution; (5) the median values with 90% credible intervals of r -band apparent magnitude distribution; (6) the GRB detection probability by considering the jet core opening angles of $\theta_c = 3.5^\circ$ and 7° .

lar momentum transport. According to some numerical simulation results (e.g., Fernández et al. 2015; Just et al. 2015; Siegel & Metzger 2017), neutrino-driven ejecta and viscosity-driven ejecta can have masses of $\sim 1\%$ and $\sim 20\%$ of the disk mass, respectively, with the root-mean-square velocities of $\sim 0.03c$ and $\sim 0.667c$. We set the gray opacities of neutrino-driven ejecta, and viscosity-driven ejecta as $1\text{ cm}^2\text{g}^{-1}$, $5\text{ cm}^2\text{g}^{-1}$, and $20\text{ cm}^2\text{g}^{-1}$ (Tanaka et al. 2020).

We use the detailed viewing-angle-dependent BHNS kilonova model presented by Zhu et al. (2020), which is essentially consistent with other models and simulations in the literature (e.g., Kawaguchi et al. 2016, 2020; Barbieri et al. 2019; Darbha et al. 2021; Zhu et al. 2022a; Gompertz et al. 2023), to simulate multi-band lightcurves of kilonova associated with BHNS GWs. The input parameters include binary parameters (M_{BH} , M_{NS} , and $\chi_{\text{BH},z}$) which can be obtained from the GW

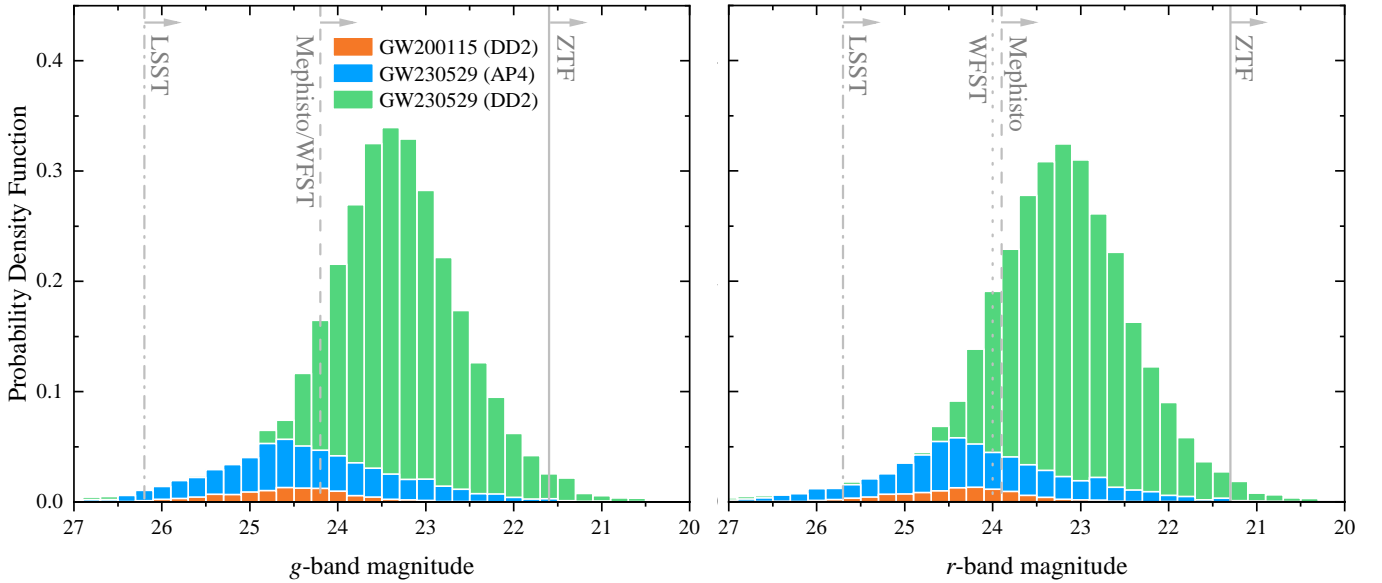


Figure 4. Probability density distributions of BHNS merger kilonova g -band (left panel) and r -band (right panel) peak magnitude for GW200115 and GW230529. The orange histograms represent the probability density for GW200115 with the consideration of the AP4 EoS, while the blue and green histograms show the probability densities for GW230529, employing the AP4 and DD2 EoSs, respectively. The gray solid, dashed, dotted, and dashed-dotted lines show the threshold depths of ZTF, Mephisto, WFST, and LSST for an exposure time of 300 s under the ideal observing conditions (Zhu et al. 2023). Here, the bin width of the histograms is set as $\Delta = 0.2$ mag.

posterior results, EoS (i.e., AP4 and DD2), luminosity distance D_L , redshift z , and two viewing angle parameters (including the latitudinal viewing angle θ_{view} and the longitudinal viewing angle φ_{view}). Here θ_{view} equals the zenith angle between the total angular momentum and the line of sight θ_{JN} inferred from the observations of GW230529, while φ_{view} is randomly simulated between 0 and 2π .

In Figure 4, we show the probability density distributions of g - and r -band peak apparent magnitudes for the GW230529 kilonova. The medians with 90% credible intervals of the peak magnitude distributions are listed in Table 2. We also mark the threshold depths of four representative survey projects, including the Zwicky Transient Facility (ZTF; Bellm et al. 2019), the Multi-channel Photometric Survey Telescope (Mephisto²), the Wide Field Survey Telescope (WFST; Wang et al. 2023) and the Large Synoptic Survey Telescope (LSST; LSST Science Collaboration et al. 2009), for an exposure time of 300 s in Figure 4. The peak apparent magnitudes of the GW230529 kilonova exhibit broad distributions with the medians of ~ 24.3 mag and ~ 23.3 mag when adopting the EoSs of AP4 and DD2, respectively. The medians of apparent magnitude distribution for DD2 are 1 mag brighter than those of GW200115, because GW230529 with $D_L = 197_{-96}^{+107}$ Mpc

is much closer than GW200115 with $D_L = 310_{-110}^{+150}$ Mpc. Even though when considering a stiff EoS of DD2, we can find that ZTF could have a limited probability of observing the kilonova emission associated with GW230529. However, operational survey projects, including Mephisto and WFST, as well as future LSST can have enough detectability to discover the GW230529 kilonova if GW230529 can make tidal disruption.

3.3. GRB Properties

We adopt a single-Gaussian structured jet model (Zhang & Mészáros 2002) to describe the GRB angular distributions of the jet kinetic energy and Lorentz factor, i.e.,

$$\begin{aligned} \frac{dE}{d\Omega}(\theta) &= \varepsilon_c \exp\left(-\frac{\theta^2}{2\theta_c^2}\right), \\ \Gamma(\theta) &= \Gamma_c \exp\left(-\frac{\theta^2}{2\theta_c^2}\right) + 1, \end{aligned} \quad (2)$$

where Γ_c is the jet core Lorentz factor, θ_c is the jet core opening angle, $\varepsilon_c \approx E_{K,\text{jet}}/2\pi\theta_c^2$, and the kinetic energy of the Blandford-Znajek jet (Blandford & Znajek 1977) is $E_{K,\text{jet}} = \epsilon(1 - \xi)M_{\text{disk}}c^2\Omega_{\text{H}}^2 f(\Omega_{\text{H}})$ with $\epsilon \approx 0.015$ following Barbieri et al. (2019), the disk mass loss ratio $\xi \approx 0.2$ (Fernández et al. 2015; Just et al. 2015; Siegel & Metzger 2017), the dimensionless angular frequency at the BH horizon $\Omega_{\text{H}} = \chi_{\text{BH},f}/2 \left(1 + \sqrt{1 - \chi_{\text{BH},f}^2}\right)$, the dimensionless spin of the final BH $\chi_{\text{BH},f}$ calculated by

² <http://www.mephisto.ynu.edu.cn>

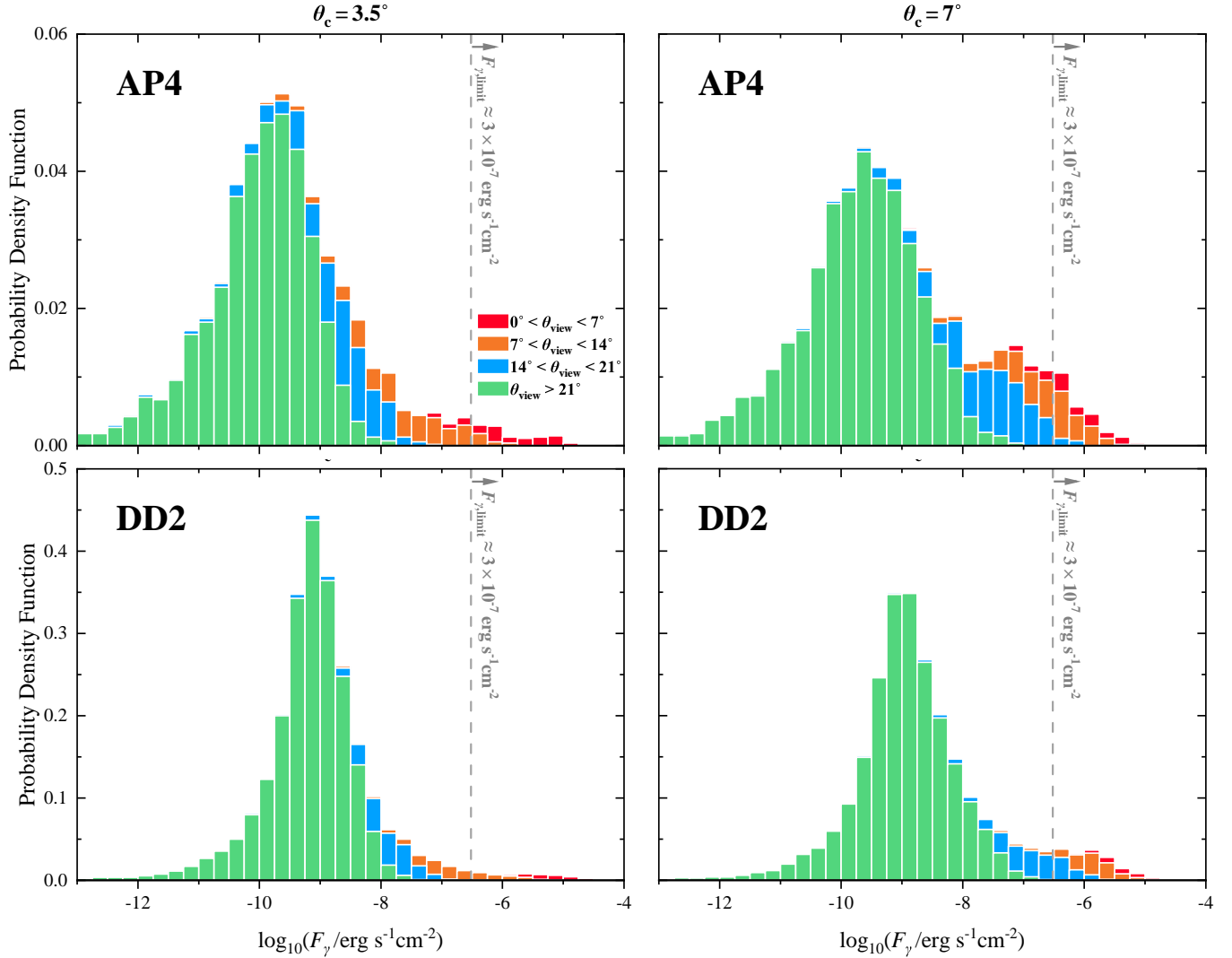


Figure 5. Probability density distributions of BHNS merger GRB γ -ray flux for GW230529. Two different core opening angles are considered: $\theta_c = 3.5^\circ$ (left panels) and 7° , as well as two EoSs, namely AP4 (top panels) and DD2 (bottom panels). The red, orange, blue, and green histograms represent GRB with latitudinal viewing angle ranges of $\theta_{\text{view}} < 7^\circ$, $7^\circ < \theta_{\text{view}} < 14^\circ$, $14^\circ < \theta_{\text{view}} < 21^\circ$, and $> 21^\circ$, respectively. The gray dashed lines indicate the effective sensitivity limit for γ -ray detectors. We note that the y -axis scalings differ between the top and bottom panels.

using Equation (11) from Pannarale (2013), and the high-spin correction $f(\Omega_{\text{H}}) = 1 + 1.38\Omega_{\text{H}}^2 - 9.2\Omega_{\text{H}}^4$. The isotropic equivalent energy of the GRB prompt emission is given by (Salafia et al. 2015)

$$E_{\gamma,\text{iso}} = \eta_{\gamma} \int \frac{dE/d\Omega}{\Gamma^4(1 - \beta \cos \alpha)^3} d\Omega(\theta, \varphi), \quad (3)$$

where the radiation efficiency is typically adopted to $\eta_{\gamma} = 0.1$, $\beta = (1 - \Gamma^{-2})^{1/2}$, $\cos \alpha = \cos \theta \cos \theta_{\text{view}} + \sin \theta \sin \theta_{\text{view}} \cos \varphi$. Therefore, we can obtain the γ -ray flux by $F_{\gamma} = E_{\gamma,\text{iso}}/4\pi D_L^2 t_j$, where the jet duration is set to $t_j \approx 1\text{s}$. Here, the GRB jet from BHNS mergers is assumed to be always launched towards the orbital angular momentum direction.

Based on the observations of both prompt and after-glow emissions from GW170817, we assume that the jet core Lorentz factor and opening angle are $\Gamma_c \sim 500$ and $\theta_c \sim 3.5^\circ$ (e.g., Lyman et al. 2018; Troja et al. 2020; Cao et al. 2023), respectively. Furthermore, because the amount of ejecta along the polar direction of BHNS mergers is typically much less than that of BNS mergers, the jets from BHNS mergers might not be effectively collimated. Therefore, we explore the variation of the jet core opening angle of $\theta_c = 7^\circ$, assessing its influence on the detection of GRBs associated with GW230529.

The viewing angle of GW230529 inferred by the LVK Collaboration is $\theta_{\text{view}} = 39_{-26}^{+33}$, suggesting that the associated GRB could be more likely an off-axis event. Based on this inferred viewing angle distribution, we

model the γ -ray flux distributions of GRB associated with GW230529 by considering two EoSs in Figure 5. The GRBs with flux larger than the effective sensitivity limit in $1 - 10^4$ keV for Swift-BAT (Gehrels et al. 2004) and SVOM-ECLAIRS (Götz et al. 2014), i.e., $F_{\gamma, \text{limit}} \sim 3 \times 10^{-7} \text{erg s}^{-1} \text{cm}^{-2}$ (Song et al. 2019), are assumed to be triggered by GRB detectors. The detection probabilities of associated GRBs for GW200115 and GW230529 are listed in Table 2.

As shown in Figure 5, the flux distributions of GW230529-associated GRB are mostly much lower than the γ -ray sensitivity limit, peaking at $\sim 10^{-10} - 10^{-9} \text{erg s}^{-1} \text{cm}^{-2}$. If $\theta_c = 3.5^\circ$, GRB detection typically requires viewing angles of $\theta_{\text{view}} < 7 - 14^\circ$; if $\theta_c = 7^\circ$, the allowed viewing angles can be slightly larger with $\theta_{\text{view}} < 14 - 21^\circ$. When adopting an EoS of AP4, the probabilities of GRB detection could be always lower than 1%. By considering the stiffer EoS of DD2, more BHNS mergers can have tidal disruption, leading to a more massive disk and hence brighter GRBs. Nevertheless, since the GW observation suggested that GW230529 was likely to be an off-axis event, the detection of its associated GRB remains challenging. When adopting $\theta_c = 3.5^\circ$, the probability of GRB detection could be as low as 1.35%. Increasing θ_c to 7° can raise the detection probability to 4.61%. If GW230529 is a disrupted event, one may conclude that the absence of a detected GRB associated with GW230529 is likely due to it being an off-axis event, as indicated by the GW observation.

3.4. Implication of EM detectability for BHNS Mergers

In the standard binary evolution scenario, most BHs typically formed at wide orbits are expected to usually possess low spins (Qin et al. 2018; Fuller et al. 2019; Belczynski et al. 2020; Mandel & Smith 2021). BHs with high orbital aligned spin in BHNS mergers can originate from tidal-induced spin-up (e.g., Qin et al. 2018; Bavera et al. 2020; Hu et al. 2022; Chattopadhyay et al. 2022) or accretion-induced spin-up (e.g., Wang et al. 2024; King et al. 2024; Zhu et al. 2024), which may only account for a small fraction of BHNS mergers. For simplicity, we assume that the spins of BHs in our simulated BHNS mergers are near-zero. Furthermore, we randomly generate $\sin\theta_{\text{view}}$ and φ_{view} within the ranges of $[0, 1]$ and $[0, 2\pi]$, respectively, for these simulated events. In Figure 2, we show the mass distribution of our population synthesis simulations introduced in Section 2.2, as well as the tidal disruption region for BHNS mergers with non-spinning BH components. One can see that BHNS mergers located in the highest probability region are always allowed to have tidal disruption. When considering

the NS EoS of AP4, all BHNS mergers with BH mass higher than the mass gap are solely plunging events, whereas tidal disruption can only happen for mergers between an mgBH and a $\lesssim 1.4 M_\odot$ NS. For the stiffer EoS of DD2, a fraction of NSs with masses $\lesssim 1.4 M_\odot$ can be tidally disrupted by $5 - 8 M_\odot$ BHs. However, mgBHNS mergers would still be the dominant events causing disruption.

Based on our population synthesis simulation results, we then simulate the tidal disruption probability, kilonova detectable rate, and GRB detection rate for GW BHNS mergers detected in the near future GW observing era (e.g., O4b and O5). We conservatively consider BHNS mergers occurring within 300 Mpc, which is the observed distance of GW200105 and GW200115, as well as the representative distance of detectable BHNS mergers in O4 (Abbott et al. 2018b; Zhu et al. 2021b; Colombo et al. 2023; Gupta et al. 2023). We find that 100% and $\gtrsim 90\%$ disrupted BHNS mergers are expected to originate from mgBHNS mergers by adopting the EoS of AP4 and DD2, respectively. When the detection depth exceeds 24 mag, the survey projects can cover the majority of kilonovae associated with BHNS mergers. However, considering the rapid rise and decline of kilonovae, their signals may be challenging to be identified. Additionally, we find that the detection rate of GRBs originating from mgBHNS mergers is $\sim 1 \text{yr}^{-1}$. Therefore, in the future, it may be possible to search for kilonova signals via the target-of-opportunity follow-up observations of both GW and GRB triggers, like the multimessenger observations between GW170817/GRB170817A/AT2017gfo.

4. CONCLUSION

In this *Letter*, we use COMPAS to explore the formation of GW230529, which is a mgBHNS merger between a $3.6_{-1.2}^{+0.7} M_\odot$ BH and a $1.43_{-0.19}^{+0.59} M_\odot$ NS reported by the LVK Collaboration. By adopting the ‘delayed’ SN prescription, our population synthesis simulations can simultaneously match the inferred event rate densities of GW230529-like mgBHNS and the total BHNS mergers, along with the population distribution of the BH mass in BHNS mergers modeled by the LVK Collaboration. The mass posterior of GW230529 significantly overlaps with the highest probability region of the simulated BHNS population. Thus, we suggest that GW230529 could originate from the isolated binary evolution channel.

By considering two specific EoSs of AP4 and DD2, the probabilities that GW230529 can have tidal disruption are 12.8% and 63.2%, respectively. If GW230529 is a disrupted event, the associated kilonova is predicted to have an apparent magnitude of $\sim 23 - 24$ mag, and

Table 3. EM Detectability of BHNS Mergers in 300 Mpc

EoS	Population	P_{tidal}	$R_{\text{tidal}}/\text{yr}^{-1}$	$R_{\text{kilonova}}/\text{yr}^{-1}$			$R_{\text{GRB}}/\text{yr}^{-1}$	
				22 mag	24 mag	26 mag	$\theta_c = 3.5^\circ$	$\theta_c = 7^\circ$
AP4	Mass-gap BHNS	32.8%	3.34	0.05	0.69	3.28	0.61	0.94
	High-mass BHNS	0	0	0	0	0	0	0
	Total BHNS	32.8%	3.34	0.05	0.69	3.28	0.61	0.94
DD2	Mass-gap BHNS	45.0%	4.58	0.27	3.59	4.55	0.91	1.41
	High-mass BHNS	3.0%	0.31	0	0.13	0.29	0.02	0.03
	Total BHNS	48.0%	4.89	0.27	3.72	4.84	0.93	1.44

NOTE—The columns are (1) the selected EoS; (2) the BHNS population, including mgBHNS mergers, high-mass BHNS mergers with BH mass of $\gtrsim 5 M_\odot$, and total BHNS mergers (3) the tidal disruption probability; (4) the tidal disruption rate in 300 Mpc; (5) the g -band kilonova detectable rate of BHNS mergers in 300 Mpc for three different detection depths of $m_g = 22, 24$, and 26 mag; (6) the detection rate of GRBs from BHNS mergers in 300 Mpc by considering two jet core opening angles of $\theta_c = 3.5^\circ$ and 7° .

hence, can be detected by the present survey projects and the LSST in the future. Since GW230529 could be an off-axis event inferred from the GW observation, its associated GRB might be too dim to be observed by γ -ray detectors, interpreting the lack of a detected GRB associated with the event.

The discovery of GW230529 revealed that the mass gap between $\sim 2.2 - 5 M_\odot$ may not exist. Previous studies indicated that most cosmological BHNS mergers involving BH masses of $\gtrsim 5 M_\odot$ are usually hard to make tidal disruption and to generate bright EM signals (e.g., Zhu et al. 2021a,b, 2022b; Fragione 2021; Drozda et al. 2022). The existence of mgBHNS mergers suggests that BHNS mergers are still likely to be multimessenger sources that emit GWs, GRBs, and kilonovae. Although mgBHNS mergers account for $\sim 60\%$ of the cosmological BHNS population, we find that 100% and $\gtrsim 90\%$ disrupted BHNS mergers are expected to originate from mgBHNS mergers, when considering the EoSs of AP4 and DD2, respectively.

Software: COMPAS, (Team COMPAS: Riley, J. et al. 2022); Python, <https://www.python.org>; Matlab, <https://www.mathworks.com>; OriginPro, <https://www.originlab.com/originpro>

ACKNOWLEDGMENTS

We thank Paul D. Lasky, Liang-Duan Liu, Ilya Mandel, Eric Thrane, Xiangyu Ivy Wang, and Yun-Wei Yu for helpful discussions. JPZ thanks the COMPAS group at Monash University. YK and LS were supported by the Beijing Natural Science Foundation (1242018), the National SKA Program of China (2020SKA0120300), and the Max Planck Partner Group Program funded by the Max Planck Society. YQ acknowledges the support of the Key Laboratory for Relativistic Astrophysics at Guangxi University.

REFERENCES

- Abbott, B. P., Abbott, R., Abbott, T. D., et al. 2017a, PhRvL, 119, 161101, doi: [10.1103/PhysRevLett.119.161101](https://doi.org/10.1103/PhysRevLett.119.161101)
- . 2017b, ApJL, 848, L13, doi: [10.3847/2041-8213/aa920c](https://doi.org/10.3847/2041-8213/aa920c)
- . 2017c, ApJL, 848, L12, doi: [10.3847/2041-8213/aa91c9](https://doi.org/10.3847/2041-8213/aa91c9)
- . 2018a, PhRvL, 121, 161101, doi: [10.1103/PhysRevLett.121.161101](https://doi.org/10.1103/PhysRevLett.121.161101)
- . 2018b, Living Reviews in Relativity, 21, 3, doi: [10.1007/s41114-018-0012-9](https://doi.org/10.1007/s41114-018-0012-9)
- . 2019, Physical Review X, 9, 011001, doi: [10.1103/PhysRevX.9.011001](https://doi.org/10.1103/PhysRevX.9.011001)
- Abbott, R., Abbott, T. D., Abraham, S., et al. 2020, ApJL, 896, L44, doi: [10.3847/2041-8213/ab960f](https://doi.org/10.3847/2041-8213/ab960f)
- . 2021a, ApJL, 915, L5, doi: [10.3847/2041-8213/ac082e](https://doi.org/10.3847/2041-8213/ac082e)
- . 2021b, Physical Review X, 11, 021053, doi: [10.1103/PhysRevX.11.021053](https://doi.org/10.1103/PhysRevX.11.021053)
- Abbott, R., Abbott, T. D., Acernese, F., et al. 2023, Physical Review X, 13, 041039, doi: [10.1103/PhysRevX.13.041039](https://doi.org/10.1103/PhysRevX.13.041039)
- Abbott, R., Abbott, T. D., Acernese, F., et al. 2023, Physical Review X, 13, 011048, doi: [10.1103/PhysRevX.13.011048](https://doi.org/10.1103/PhysRevX.13.011048)

- Acernese, F., Agathos, M., Agatsuma, K., et al. 2015, *Classical and Quantum Gravity*, 32, 024001, doi: [10.1088/0264-9381/32/2/024001](https://doi.org/10.1088/0264-9381/32/2/024001)
- Akmal, A., & Pandharipande, V. R. 1997, *PhRvC*, 56, 2261, doi: [10.1103/PhysRevC.56.2261](https://doi.org/10.1103/PhysRevC.56.2261)
- Alsing, J., Silva, H. O., & Berti, E. 2018, *MNRAS*, 478, 1377, doi: [10.1093/mnras/sty1065](https://doi.org/10.1093/mnras/sty1065)
- Anand, S., Coughlin, M. W., Kasliwal, M. M., et al. 2021, *Nature Astronomy*, 5, 46, doi: [10.1038/s41550-020-1183-3](https://doi.org/10.1038/s41550-020-1183-3)
- Andrews, J. J., Taggart, K., & Foley, R. 2022, arXiv e-prints, arXiv:2207.00680, doi: [10.48550/arXiv.2207.00680](https://doi.org/10.48550/arXiv.2207.00680)
- Antoniadis, J., Freire, P. C. C., Wex, N., et al. 2013, *Science*, 340, 448, doi: [10.1126/science.1233232](https://doi.org/10.1126/science.1233232)
- Arcavi, I., Hosseinzadeh, G., Howell, D. A., et al. 2017, *Nature*, 551, 64, doi: [10.1038/nature24291](https://doi.org/10.1038/nature24291)
- Aso, Y., Michimura, Y., Somiya, K., et al. 2013, *PhRvD*, 88, 043007, doi: [10.1103/PhysRevD.88.043007](https://doi.org/10.1103/PhysRevD.88.043007)
- Atri, P., Miller-Jones, J. C. A., Bahramian, A., et al. 2019, *MNRAS*, 489, 3116, doi: [10.1093/mnras/stz2335](https://doi.org/10.1093/mnras/stz2335)
- Bailyn, C. D., Jain, R. K., Coppi, P., & Orosz, J. A. 1998, *ApJ*, 499, 367, doi: [10.1086/305614](https://doi.org/10.1086/305614)
- Barbieri, C., Salafia, O. S., Perego, A., Colpi, M., & Ghirlanda, G. 2019, *A&A*, 625, A152, doi: [10.1051/0004-6361/201935443](https://doi.org/10.1051/0004-6361/201935443)
- Bardeen, J. M., Press, W. H., & Teukolsky, S. A. 1972, *ApJ*, 178, 347, doi: [10.1086/151796](https://doi.org/10.1086/151796)
- Bavera, S. S., Fragos, T., Qin, Y., et al. 2020, *A&A*, 635, A97, doi: [10.1051/0004-6361/201936204](https://doi.org/10.1051/0004-6361/201936204)
- Belczynski, K., Kléncki, J., Fields, C. E., et al. 2020, *A&A*, 636, A104, doi: [10.1051/0004-6361/201936528](https://doi.org/10.1051/0004-6361/201936528)
- Bellm, E. C., Kulkarni, S. R., Graham, M. J., et al. 2019, *PASP*, 131, 018002, doi: [10.1088/1538-3873/aaecbe](https://doi.org/10.1088/1538-3873/aaecbe)
- Biscoveanu, S., Landry, P., & Vitale, S. 2023, *MNRAS*, 518, 5298, doi: [10.1093/mnras/stac3052](https://doi.org/10.1093/mnras/stac3052)
- Blandford, R. D., & Znajek, R. L. 1977, *MNRAS*, 179, 433, doi: [10.1093/mnras/179.3.433](https://doi.org/10.1093/mnras/179.3.433)
- Broekgaarden, F. S., & Berger, E. 2021, *ApJL*, 920, L13, doi: [10.3847/2041-8213/ac2832](https://doi.org/10.3847/2041-8213/ac2832)
- Broekgaarden, F. S., Berger, E., Neijssel, C. J., et al. 2021, *MNRAS*, 508, 5028, doi: [10.1093/mnras/stab2716](https://doi.org/10.1093/mnras/stab2716)
- Cao, X.-F., Tan, W.-W., Yu, Y.-W., & Zhang, Z.-D. 2023, arXiv e-prints, arXiv:2306.16795, doi: [10.48550/arXiv.2306.16795](https://doi.org/10.48550/arXiv.2306.16795)
- Chattopadhyay, D., Stevenson, S., Broekgaarden, F., Antonini, F., & Belczynski, K. 2022, *MNRAS*, 513, 5780, doi: [10.1093/mnras/stac1283](https://doi.org/10.1093/mnras/stac1283)
- Colombo, A., Duqué, R., Sharan Salafia, O., et al. 2023, arXiv e-prints, arXiv:2310.16894, doi: [10.48550/arXiv.2310.16894](https://doi.org/10.48550/arXiv.2310.16894)
- Coughlin, M., Dietrich, T., Kawaguchi, K., et al. 2017, *ApJ*, 849, 12, doi: [10.3847/1538-4357/aa9114](https://doi.org/10.3847/1538-4357/aa9114)
- Coughlin, M. W., Dietrich, T., Antier, S., et al. 2020, *MNRAS*, 497, 1181, doi: [10.1093/mnras/staa1925](https://doi.org/10.1093/mnras/staa1925)
- Coulter, D. A., Foley, R. J., Kilpatrick, C. D., et al. 2017, *Science*, 358, 1556, doi: [10.1126/science.aap9811](https://doi.org/10.1126/science.aap9811)
- Darbha, S., Kasen, D., Foucart, F., & Price, D. J. 2021, *ApJ*, 915, 69, doi: [10.3847/1538-4357/abff5d](https://doi.org/10.3847/1538-4357/abff5d)
- D’Orazio, D. J., Haiman, Z., Levin, J., Samsing, J., & Vigna-Gómez, A. 2022, *ApJ*, 927, 56, doi: [10.3847/1538-4357/ac4bdb](https://doi.org/10.3847/1538-4357/ac4bdb)
- Drout, M. R., Piro, A. L., Shappee, B. J., et al. 2017, *Science*, 358, 1570, doi: [10.1126/science.aaq0049](https://doi.org/10.1126/science.aaq0049)
- Drozda, P., Belczynski, K., O’Shaughnessy, R., Bulik, T., & Fryer, C. L. 2022, *A&A*, 667, A126, doi: [10.1051/0004-6361/202039418](https://doi.org/10.1051/0004-6361/202039418)
- Eichler, D., Livio, M., Piran, T., & Schramm, D. N. 1989, *Nature*, 340, 126, doi: [10.1038/340126a0](https://doi.org/10.1038/340126a0)
- Evans, P. A., Cenko, S. B., Kennea, J. A., et al. 2017, *Science*, 358, 1565, doi: [10.1126/science.aap9580](https://doi.org/10.1126/science.aap9580)
- Farr, W. M., Sravan, N., Cantrell, A., et al. 2011, *ApJ*, 741, 103, doi: [10.1088/0004-637X/741/2/103](https://doi.org/10.1088/0004-637X/741/2/103)
- Fernández, R., Kasen, D., Metzger, B. D., & Quataert, E. 2015, *MNRAS*, 446, 750, doi: [10.1093/mnras/stu2112](https://doi.org/10.1093/mnras/stu2112)
- Foucart, F. 2012, *PhRvD*, 86, 124007, doi: [10.1103/PhysRevD.86.124007](https://doi.org/10.1103/PhysRevD.86.124007)
- Foucart, F., Hinderer, T., & Nissanke, S. 2018, *PhRvD*, 98, 081501, doi: [10.1103/PhysRevD.98.081501](https://doi.org/10.1103/PhysRevD.98.081501)
- Fragione, G. 2021, *ApJL*, 923, L2, doi: [10.3847/2041-8213/ac3bcd](https://doi.org/10.3847/2041-8213/ac3bcd)
- Fryer, C. L., Belczynski, K., Wiktorowicz, G., et al. 2012, *ApJ*, 749, 91, doi: [10.1088/0004-637X/749/1/91](https://doi.org/10.1088/0004-637X/749/1/91)
- Fuller, J., Piro, A. L., & Jermyn, A. S. 2019, *MNRAS*, 485, 3661, doi: [10.1093/mnras/stz514](https://doi.org/10.1093/mnras/stz514)
- Gao, H., Ai, S.-K., Cao, Z.-J., et al. 2020, *Frontiers of Physics*, 15, 24603, doi: [10.1007/s11467-019-0945-9](https://doi.org/10.1007/s11467-019-0945-9)
- Gehrels, N., Chincarini, G., Giommi, P., et al. 2004, *ApJ*, 611, 1005, doi: [10.1086/422091](https://doi.org/10.1086/422091)
- Goldstein, A., Veres, P., Burns, E., et al. 2017, *ApJL*, 848, L14, doi: [10.3847/2041-8213/aa8f41](https://doi.org/10.3847/2041-8213/aa8f41)
- Gompertz, B. P., Nicholl, M., Smith, J. C., et al. 2023, *MNRAS*, 526, 4585, doi: [10.1093/mnras/stad2990](https://doi.org/10.1093/mnras/stad2990)
- Gompertz, B. P., Cutter, R., Steeghs, D., et al. 2020, *MNRAS*, 497, 726, doi: [10.1093/mnras/staa1845](https://doi.org/10.1093/mnras/staa1845)
- Gottlieb, O., Issa, D., Jacquemin-Ide, J., et al. 2023, *ApJL*, 954, L21, doi: [10.3847/2041-8213/aceeff](https://doi.org/10.3847/2041-8213/aceeff)

- Götz, D., Osborne, J., Cordier, B., et al. 2014, in Society of Photo-Optical Instrumentation Engineers (SPIE) Conference Series, Vol. 9144, Space Telescopes and Instrumentation 2014: Ultraviolet to Gamma Ray, ed. T. Takahashi, J.-W. A. den Herder, & M. Bautz, 914423, doi: [10.1117/12.2054898](https://doi.org/10.1117/12.2054898)
- Gupta, I., Borhanian, S., Dhani, A., et al. 2023, PhRvD, 107, 124007, doi: [10.1103/PhysRevD.107.124007](https://doi.org/10.1103/PhysRevD.107.124007)
- Hayashi, K., Kawaguchi, K., Kiuchi, K., Kyutoku, K., & Shibata, M. 2021, PhRvD, 103, 043007, doi: [10.1103/PhysRevD.103.043007](https://doi.org/10.1103/PhysRevD.103.043007)
- Hobbs, G., Lorimer, D. R., Lyne, A. G., & Kramer, M. 2005, MNRAS, 360, 974, doi: [10.1111/j.1365-2966.2005.09087.x](https://doi.org/10.1111/j.1365-2966.2005.09087.x)
- Hu, R.-C., Zhu, J.-P., Qin, Y., et al. 2022, ApJ, 928, 163, doi: [10.3847/1538-4357/ac573f](https://doi.org/10.3847/1538-4357/ac573f)
- Just, O., Bauswein, A., Ardevol Pulpillo, R., Goriely, S., & Janka, H. T. 2015, MNRAS, 448, 541, doi: [10.1093/mnras/stv009](https://doi.org/10.1093/mnras/stv009)
- Kasen, D., Metzger, B., Barnes, J., Quataert, E., & Ramirez-Ruiz, E. 2017, Nature, 551, 80, doi: [10.1038/nature24453](https://doi.org/10.1038/nature24453)
- Kasliwal, M. M., Nakar, E., Singer, L. P., et al. 2017, Science, 358, 1559, doi: [10.1126/science.aap9455](https://doi.org/10.1126/science.aap9455)
- Kasliwal, M. M., Anand, S., Ahumada, T., et al. 2020, ApJ, 905, 145, doi: [10.3847/1538-4357/abc335](https://doi.org/10.3847/1538-4357/abc335)
- Kawaguchi, K., Kyutoku, K., Shibata, M., & Tanaka, M. 2016, ApJ, 825, 52, doi: [10.3847/0004-637X/825/1/52](https://doi.org/10.3847/0004-637X/825/1/52)
- Kawaguchi, K., Shibata, M., & Tanaka, M. 2020, ApJ, 889, 171, doi: [10.3847/1538-4357/ab61f6](https://doi.org/10.3847/1538-4357/ab61f6)
- Kilpatrick, C. D., Foley, R. J., Kasen, D., et al. 2017, Science, 358, 1583, doi: [10.1126/science.aaq0073](https://doi.org/10.1126/science.aaq0073)
- Kyutoku, K., Ioka, K., Okawa, H., Shibata, M., & Taniguchi, K. 2015, PhRvD, 92, 044028, doi: [10.1103/PhysRevD.92.044028](https://doi.org/10.1103/PhysRevD.92.044028)
- Kyutoku, K., Ioka, K., & Shibata, M. 2013, PhRvD, 88, 041503, doi: [10.1103/PhysRevD.88.041503](https://doi.org/10.1103/PhysRevD.88.041503)
- Li, L.-X., & Paczyński, B. 1998, ApJL, 507, L59, doi: [10.1086/311680](https://doi.org/10.1086/311680)
- LIGO Scientific Collaboration, Aasi, J., Abbott, B. P., et al. 2015, Classical and Quantum Gravity, 32, 074001, doi: [10.1088/0264-9381/32/7/074001](https://doi.org/10.1088/0264-9381/32/7/074001)
- LSST Science Collaboration, Abell, P. A., Allison, J., et al. 2009, arXiv e-prints, arXiv:0912.0201, doi: [10.48550/arXiv.0912.0201](https://doi.org/10.48550/arXiv.0912.0201)
- Lyman, J. D., Lamb, G. P., Levan, A. J., et al. 2018, Nature Astronomy, 2, 751, doi: [10.1038/s41550-018-0511-3](https://doi.org/10.1038/s41550-018-0511-3)
- Madau, P., & Dickinson, M. 2014, ARA&A, 52, 415, doi: [10.1146/annurev-astro-081811-125615](https://doi.org/10.1146/annurev-astro-081811-125615)
- Mandel, I., & Müller, B. 2020, MNRAS, 499, 3214, doi: [10.1093/mnras/staa3043](https://doi.org/10.1093/mnras/staa3043)
- Mandel, I., & Smith, R. J. E. 2021, ApJL, 922, L14, doi: [10.3847/2041-8213/ac35dd](https://doi.org/10.3847/2041-8213/ac35dd)
- Metzger, B. D., Martínez-Pinedo, G., Darbha, S., et al. 2010, MNRAS, 406, 2650, doi: [10.1111/j.1365-2966.2010.16864.x](https://doi.org/10.1111/j.1365-2966.2010.16864.x)
- Narayan, R., Paczynski, B., & Piran, T. 1992, ApJL, 395, L83, doi: [10.1086/186493](https://doi.org/10.1086/186493)
- Neijssel, C. J., Vigna-Gómez, A., Stevenson, S., et al. 2019, MNRAS, 490, 3740, doi: [10.1093/mnras/stz2840](https://doi.org/10.1093/mnras/stz2840)
- Özel, F., Psaltis, D., Narayan, R., & McClintock, J. E. 2010, ApJ, 725, 1918, doi: [10.1088/0004-637X/725/2/1918](https://doi.org/10.1088/0004-637X/725/2/1918)
- Paczynski, B. 1986, ApJL, 308, L43, doi: [10.1086/184740](https://doi.org/10.1086/184740)
- . 1991, A&A, 41, 257
- Pannarale, F. 2013, PhRvD, 88, 104025, doi: [10.1103/PhysRevD.88.104025](https://doi.org/10.1103/PhysRevD.88.104025)
- Panter, B., Heavens, A. F., & Jimenez, R. 2004, MNRAS, 355, 764, doi: [10.1111/j.1365-2966.2004.08355.x](https://doi.org/10.1111/j.1365-2966.2004.08355.x)
- Pian, E., D’Avanzo, P., Benetti, S., et al. 2017, Nature, 551, 67, doi: [10.1038/nature24298](https://doi.org/10.1038/nature24298)
- Qin, Y., Fragos, T., Meynet, G., et al. 2018, A&A, 616, A28, doi: [10.1051/0004-6361/201832839](https://doi.org/10.1051/0004-6361/201832839)
- Rivinius, T., Baade, D., Hadrava, P., Heida, M., & Klement, R. 2020, A&A, 637, L3, doi: [10.1051/0004-6361/202038020](https://doi.org/10.1051/0004-6361/202038020)
- Romani, R. W., Kandel, D., Filippenko, A. V., Brink, T. G., & Zheng, W. 2022, ApJL, 934, L17, doi: [10.3847/2041-8213/ac8007](https://doi.org/10.3847/2041-8213/ac8007)
- Salafia, O. S., Ghisellini, G., Pescalli, A., Ghirlanda, G., & Nappo, F. 2015, MNRAS, 450, 3549, doi: [10.1093/mnras/stv766](https://doi.org/10.1093/mnras/stv766)
- Sarin, N., Lasky, P. D., Vivanco, F. H., et al. 2022, PhRvD, 105, 083004, doi: [10.1103/PhysRevD.105.083004](https://doi.org/10.1103/PhysRevD.105.083004)
- Savchenko, V., Ferrigno, C., Kuulkers, E., et al. 2017, ApJL, 848, L15, doi: [10.3847/2041-8213/aa8f94](https://doi.org/10.3847/2041-8213/aa8f94)
- Shao, Y., & Li, X.-D. 2021, ApJ, 920, 81, doi: [10.3847/1538-4357/ac173e](https://doi.org/10.3847/1538-4357/ac173e)
- Shibata, M., & Taniguchi, K. 2011, Living Reviews in Relativity, 14, 6, doi: [10.12942/lrr-2011-6](https://doi.org/10.12942/lrr-2011-6)
- Siegel, D. M., & Metzger, B. D. 2017, PhRvL, 119, 231102, doi: [10.1103/PhysRevLett.119.231102](https://doi.org/10.1103/PhysRevLett.119.231102)
- Smartt, S. J., Chen, T. W., Jerkstrand, A., et al. 2017, Nature, 551, 75, doi: [10.1038/nature24303](https://doi.org/10.1038/nature24303)
- Song, H.-R., Ai, S.-K., Wang, M.-H., et al. 2019, ApJL, 881, L40, doi: [10.3847/2041-8213/ab3921](https://doi.org/10.3847/2041-8213/ab3921)
- Stevenson, S., Vigna-Gómez, A., Mandel, I., et al. 2017, Nature Communications, 8, 14906, doi: [10.1038/ncomms14906](https://doi.org/10.1038/ncomms14906)

- Tanaka, M., Kato, D., Gaigalas, G., & Kawaguchi, K. 2020, MNRAS, 496, 1369, doi: [10.1093/mnras/staa1576](https://doi.org/10.1093/mnras/staa1576)
- Team COMPAS: Riley, J., Agrawal, P., Barrett, J. W., et al. 2022, ApJS, 258, 34, doi: [10.3847/1538-4365/ac416c](https://doi.org/10.3847/1538-4365/ac416c)
- The LIGO Scientific Collaboration, the Virgo Collaboration, & the KAGRA Collaboration. 2024, arXiv e-prints, arXiv:2404.04248, <https://arxiv.org/abs/2404.04248>
- The LIGO Scientific Collaboration, the Virgo Collaboration, Abbott, R., et al. 2021, arXiv e-prints, arXiv:2108.01045, doi: [10.48550/arXiv.2108.01045](https://doi.org/10.48550/arXiv.2108.01045)
- Thompson, T. A., Kochanek, C. S., Stanek, K. Z., et al. 2019, Science, 366, 637, doi: [10.1126/science.aau4005](https://doi.org/10.1126/science.aau4005)
- Troja, E., van Eerten, H., Zhang, B., et al. 2020, MNRAS, 498, 5643, doi: [10.1093/mnras/staa2626](https://doi.org/10.1093/mnras/staa2626)
- Typel, S., Röpke, G., Klähn, T., Blaschke, D., & Wolter, H. H. 2010, PhRvC, 81, 015803, doi: [10.1103/PhysRevC.81.015803](https://doi.org/10.1103/PhysRevC.81.015803)
- Vigna-Gómez, A., Neijssel, C. J., Stevenson, S., et al. 2018, MNRAS, 481, 4009, doi: [10.1093/mnras/sty2463](https://doi.org/10.1093/mnras/sty2463)
- Wang, T., Liu, G., Cai, Z., et al. 2023, Science China Physics, Mechanics, and Astronomy, 66, 109512, doi: [10.1007/s11433-023-2197-5](https://doi.org/10.1007/s11433-023-2197-5)
- Wang, Z.-H.-T., Hu, R.-C., Qin, Y., et al. 2024, arXiv e-prints, arXiv:2401.17558, doi: [10.48550/arXiv.2401.17558](https://doi.org/10.48550/arXiv.2401.17558)
- Wyrzykowski, L., & Mandel, I. 2020, A&A, 636, A20, doi: [10.1051/0004-6361/201935842](https://doi.org/10.1051/0004-6361/201935842)
- Xing, Z., Bavera, S. S., Fragos, T., et al. 2024, A&A, 683, A144, doi: [10.1051/0004-6361/202347971](https://doi.org/10.1051/0004-6361/202347971)
- Ye, C., & Fishbach, M. 2022, ApJ, 937, 73, doi: [10.3847/1538-4357/ac7f99](https://doi.org/10.3847/1538-4357/ac7f99)
- Zhang, B. 2018, The Physics of Gamma-Ray Bursts (Cambridge University Press), doi: [10.1017/9781139226530](https://doi.org/10.1017/9781139226530)
- Zhang, B., & Mészáros, P. 2002, ApJ, 571, 876, doi: [10.1086/339981](https://doi.org/10.1086/339981)
- Zhang, B. B., Zhang, B., Sun, H., et al. 2018, Nature Communications, 9, 447, doi: [10.1038/s41467-018-02847-3](https://doi.org/10.1038/s41467-018-02847-3)
- Zhu, J.-P., Qin, Y., Wang, Z.-H.-T., et al. 2024, MNRAS, 529, 4554, doi: [10.1093/mnras/stae815](https://doi.org/10.1093/mnras/stae815)
- Zhu, J.-P., Wang, X. I., Sun, H., et al. 2022a, ApJL, 936, L10, doi: [10.3847/2041-8213/ac85ad](https://doi.org/10.3847/2041-8213/ac85ad)
- Zhu, J.-P., Wu, S., Qin, Y., et al. 2022b, ApJ, 928, 167, doi: [10.3847/1538-4357/ac540c](https://doi.org/10.3847/1538-4357/ac540c)
- Zhu, J.-P., Wu, S., Yang, Y.-P., et al. 2021a, ApJ, 921, 156, doi: [10.3847/1538-4357/ac19a7](https://doi.org/10.3847/1538-4357/ac19a7)
- Zhu, J.-P., Yang, Y.-P., Liu, L.-D., et al. 2020, ApJ, 897, 20, doi: [10.3847/1538-4357/ab93bf](https://doi.org/10.3847/1538-4357/ab93bf)
- Zhu, J.-P., Wu, S., Yang, Y.-P., et al. 2021b, ApJ, 917, 24, doi: [10.3847/1538-4357/abfe5e](https://doi.org/10.3847/1538-4357/abfe5e)
- . 2023, ApJ, 942, 88, doi: [10.3847/1538-4357/aca527](https://doi.org/10.3847/1538-4357/aca527)